10

Double-diffusion in active environments

In fluid dynamics, the prominent place occupied by double-diffusion is perfectly secure – the indisputable beauty and intellectual challenges of the topic are more than sufficient to maintain the keen interest of dynamicists for many years to come. More applied folks, oceanographers being the prime example, are harder to please. The acceptance of double-diffusion as a core oceanographic subject is conditioned on proving, beyond reasonable doubt, its impact on water-mass composition. The final verdict rests largely on the ability of double-diffusion to remain an effective mixing process in the ocean despite the perpetual forcing by externally driven shears and turbulence. Are salt fingers sufficiently resilient to survive in such an environment? And if they do, how relevant are the good old theories developed for unforced double-diffusion? Concerns of this nature have been expressed continuously throughout the history of the field, and not only by the small and irrational group of double-diffusion haters. An early quote from the founder of the field reflects very serious reservations: "The ease with which organized salt fingers may be disrupted would seem to argue against their playing any significant role in the vertical mixing of a turbulent ocean" (Stern, 1967).

While the precise assessment is yet to be made, the evidence already accumulated suggests that external forcing in the ocean tends to reduce double-diffusive transport, but not everywhere and not dramatically. The very existence of phenomena such as permanent thermohaline staircases indicates that not only is double-diffusion active in the ocean but that it can be the dominant mixing process. Staircases are observed in regions where they are roughly expected on the basis of theoretical considerations (Chapter 8) – considerations that do not take external forcing into account. Thus, if double-diffusion is active enough to generate staircases, then waves, shear and turbulence likely play a secondary role in finescale dynamics. This is not to say that these ocean-specific effects can be dismissed entirely. As we shall see shortly, external forcing can produce detectable changes

in stratification and transport even in staircases, but it is certainly no match for double-diffusion. The situation becomes more complicated and uncertain when stratification favors double-diffusion but not necessarily layering, which is the most common situation in the mid-latitude thermocline. In this case, the fate of double-diffusion is determined by a combination of several factors, such as the value of density ratio, the intensity of ambient shear and the frequency of turbulent overturns.

The following discussion is an attempt to quantify the relative impact of various forms of external forcing on double-diffusion in both smooth-gradient and staircase regimes. Our focus is on fingering rather than diffusive convection. There are two (related) reasons for that. First, much more is known about salt fingers in active environments; the diffusive problem has so far generated less excitement and research activity. The second reason is that salt fingers are more likely to be affected by ambient forcing. Observational estimates of mixing in diffusive regions of the ocean are generally consistent with predictions based on unforced laboratory experiments, which is not always the case for salt fingers. The lack of controversy ultimately translates to a lack of interest. So, let us talk about salt fingers and let us start with the effects of shear.

10.1 The interaction of salt fingers with shear flow

Vertical shears are ubiquitous in the ocean. They are usually associated with internal waves generated by tides, topography and atmospheric forcing. Therefore, a very natural development in double-diffusion theory involves the interaction of salt fingers with shear. The first systematic study of this problem was performed by Linden (1974), whose laboratory experiments revealed that active double-diffusive convection is maintained in the presence of a steady shear flow. Using a combination of theoretical arguments and experiments, Linden demonstrated that the preferred pattern of instability is a quasi two-dimensional mode parallel to the mean flow, which was referred to as salt sheets. These remarkably regular structures can be seen very clearly in the top-view shadowgraph images of Linden's experiments (Fig. 10.1).

The interest in the role of shear in salt-finger dynamics was invigorated by the 1985 C-SALT program (Schmitt *et al.*, 1987), which brought two unexpected findings. The first one is the presence of nearly horizontal small-scale laminae (Fig. 10.2) clearly visible in the shadowgraphs taken through high-gradient interfaces (Kunze, 1990). The second surprise is very significant, an order-of-magnitude discrepancy between the observed heat fluxes and predictions based on the laboratory-calibrated Turner's 4/3 flux law (Chapter 4). Both effects are apparently related to some aspect of the external forcing and the most common off-hand

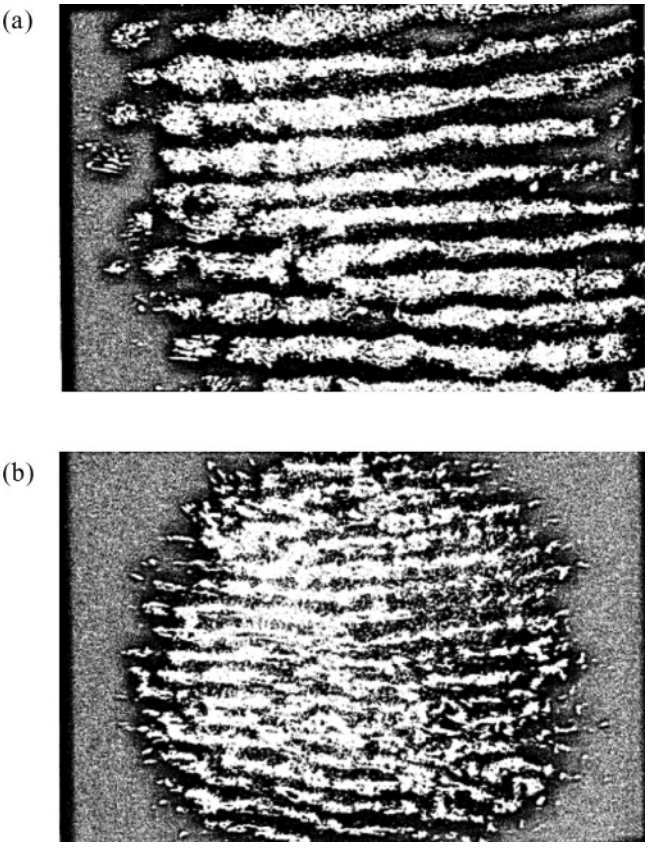

Figure 10.1 Laboratory experiment on salt fingers in steady shear flow. The top-view photographs reveal the horizontal structure of salt sheets aligned in the direction of shear. From Linden (1974).

reaction of an observer is to attribute them to the vertical shear. The strength of shear measured in C-SALT interfaces was moderate, with typical Richardson numbers of $Ri \sim 6$ (Gregg and Sanford, 1987). Shears of such strength are sufficient to tilt salt fingers and there is little doubt that inclined fingers are less effective in mixing temperature and salinity than vertical ones. However, is it reasonable to expect an order-of-magnitude reduction in fluxes, as the failure of the 4/3 flux laws seems to indicate?

Several arguments suggest that the impact of shear on finger transport is relatively mild. For instance, it is clear that while steady unidirectional shear can be effective in suppressing the along-flow variability, it cannot directly affect the cross-flow motion. The appearance of quasi two-dimensional salt sheets in Linden's (1974) experiments (Fig. 10.1) is a sign of highly anisotropic dynamics. The anisotropy

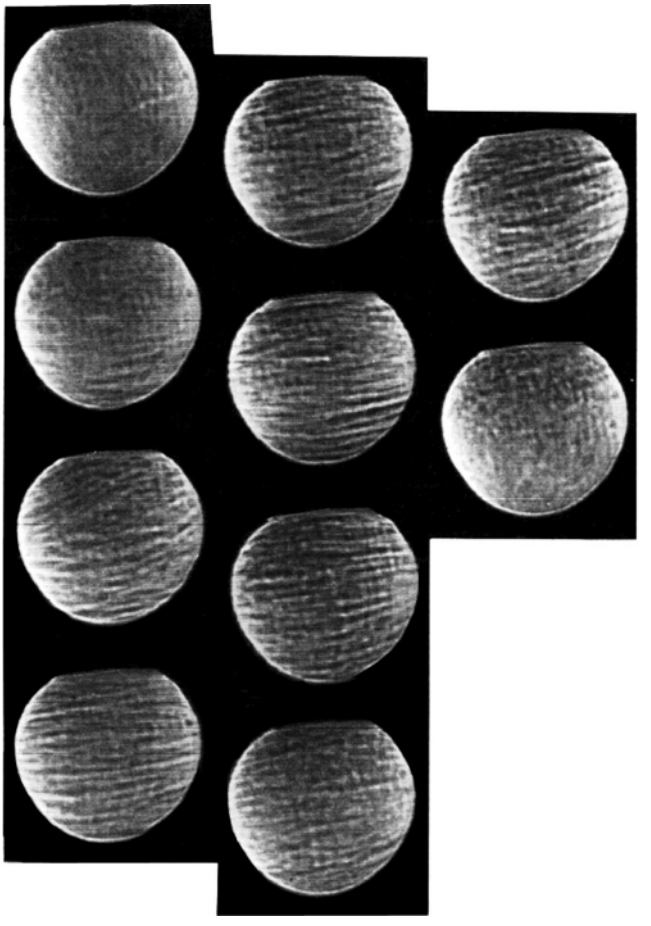

Figure 10.2 Shadowgraph images through a fingering-favorable interface of the Caribbean staircase. From Kunze (1990).

can be readily rationalized from the general structure of the governing (Navier–Stokes) equations. These equations are invariant with respect to the transformation in which patterns that are homogeneous in one spatial direction [$T = T(y, z, t)$] are augmented by a steady shear in the same direction [$u = u_{\text{shear}}(y, z)$]. Hence, shear and two-dimensional cross-shear modes are effectively uncoupled. Even if shear is strong enough to completely eliminate all downstream variability, the cross-shear modes will remain largely intact.

The quasi two-dimensional interpretation of the finger/shear dynamics is supported by numerical experiments. Figure 10.3 presents the direct numerical simulation of salt sheets by Kimura and Smyth (2011). While the cross-flow patterns are remarkably similar to salt fingers in two-dimensional simulations, the downstream

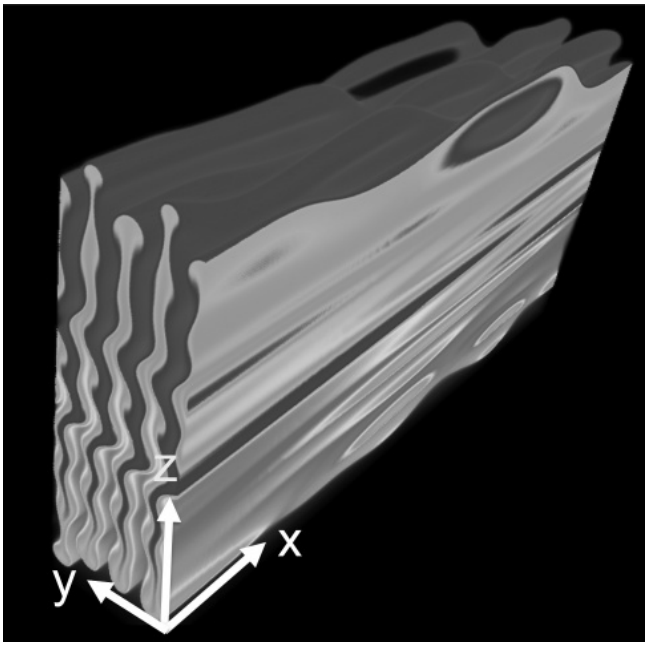

Figure 10.3 A snapshot of the salinity field from DNS initialized with four salt sheets in a background shear. From Kimura and Smyth (2011).

variability is reduced to the small-scale, nearly horizontal laminae suggestive of the shadowgraph observations in Figure 10.2. Three-dimensional simulations also indicate that salt-finger fluxes in laminar shear (Smyth and Kimura, 2007) are approximately halved relative to their unsheared counterparts and are in fact very close to two-dimensional fluxes (Stern *et al*., 2001).

Another suggestive effect observed in simulations (Kimura *et al*., 2011) and laboratory experiments (Linden, 1974; Fernandes and Krishnamurti, 2010) involves the very limited response of fingers to variation in the strength of shear. Even the sign of this response could be questioned. Linden (1974) predicted a weak increase of fluxes with increasing shear, whereas the opposite trend was reported by Kimura *et al*. (2011) and Fernandes and Krishnamurti (2010). The lack of significant flux/shear dependence is consistent with our interpretation of the zero-order physics at play. Shear rapidly makes the pattern and dynamics of salt fingers effectively two-dimensional, at which point shear and fingers stop interacting. Thus, while the presence of shear matters, its strength generally does not. The whole story is of course more complicated; the extent of downstream homogenization and secondary three-dimensional instabilities of salt sheets are of interest (Kimura and Smyth, 2011) and should be explored further. However, as far as the magnitude of double-diffusive mixing in shear is concerned, the bottom line is clear. It is unlikely

that steady shear can reduce vertical transport by more than a factor of 2–2.5 – the typical difference between finger fluxes in two and three dimensions.

An interesting idea on finger dynamics in shear was put forward by Kunze (1990), who emphasized the time dependence of a background flow. In the C-SALT staircase, as elsewhere in the ocean, shear is predominantly near-inertial. As shear makes a full rotation, it successively suppresses salt-finger variability in all horizontal directions, not just one. In this sense, rotating and steady shears are different, the former being potentially more effective in constraining double-diffusive mixing. What casts some doubt on the relevance of this mechanism is the disparity of temporal scales. While the inertial shear varies on the time scale of a day, the salt-finger growth period for C-SALT parameters is measured in minutes. It therefore appears that the steady-state approximation should be adequate, although more precise quantification of time-dependent effects is highly desirable. A straightforward and convenient way of addressing the problem would be to use direct numerical simulations, since computational capabilities are now sufficient to model salt fingers on the inertial time scales.

10.2 Low fluxes and thick interfaces

What are the other factors that could potentially reduce salt finger transport in the ocean? We have mentioned an order-of-magnitude mismatch between the predictions of the laboratory calibrated flux laws and heat flux measurements in the C-SALT staircase, which still has not been fully explained after three decades of deliberation. A similar mismatch has been noted (Hebert, 1988) for steps observed in a salt lens of Mediterranean origin (meddy Sharon). Taking into account the effects of shear reduces the inconsistency, but does not resove the problem completely. A potentially important hint (Kunze, 1987) for the too-low-flux puzzle is provided by the analysis of the interface thickness (h). The interfacial similarity law (4.8) makes it possible to estimate h based on the extrapolation of laboratory measurements and to compare it with observations. The outcome is intriguing: the typical observed thickness of C-SALT interfaces ($h \sim 2$ m) is much higher than the lab-based prediction ($h \sim 0.2$ m). This discrepancy is fully consistent with the limited T–S transport in the C-SALT staircase: thick interfaces mean weak gradients; weak gradients mean low fluxes. However, thickness analysis does not reveal the ultimate cause of the mismatch of fluxes, immediately prompting the question: "Then why are interfaces in the ocean so disproportionally thick?"

It has been suggested that, conceptually, it is more appropriate to view interfaces in the ocean as a stack of several thin sub-interfaces and that Turner's similarity laws should be applied to the sub-interfaces, rather than to the net gradient

region (e.g., Kunze, 1987). Some support for this interpretation is provided by observations of small-scale vertical non-uniformities of temperature gradient in interfaces (e.g., Molcard and Williams, 1975). The intensity of microstructure is also modulated, with the most active salt fingering restricted to regions with large temperature gradients. Such banded, horizontally coherent structures, of various strengths and patterns, have been observed in all major salt-finger staircases. The most pronounced form of the interfacial substructure is represented by "mini-staircases" with well-defined steps of 1–2 m nested within much thicker parent interfaces (Marmorino, 1989). The origin of such phenomena remains unknown.

A notable attempt to rationalize the discrepancy between the structure of oceanic and laboratory interfaces was made by Linden (1978). A distinguishing feature of laboratory experiments is the initial setup, which usually consists of two homogeneous layers separated by a sharp interface. To examine the ramifications of imposing this somewhat arbitrary initial condition, Linden conducted a series of experiments with thick interfaces. He demonstrated that, in time, such interfaces either shrink significantly or split into several interfaces separated by convecting layers. In either case, the thicknesses of individual interfaces inexorably evolved towards a certain preferred value, typically much less than the initial thickness. Linden's (1978) findings suggest that the role of initial conditions in the selection of interfacial thickness is secondary. This is an interesting result in its own right but, unfortunately, it also implies that the explanation of the difference between oceanic and laboratory interfaces lies elsewhere. One possibility is related to intermittent oceanic turbulence, which is discussed next.

10.3 The interaction with intermittent turbulence

On the qualitative level, the physics of the interaction between salt fingers and turbulence is reasonably well understood. Intermittent density overturns, induced by dynamic instabilities of internal waves, generate energetic turbulent billows. When turbulent events occur in the ocean regions occupied by fingering convection, they disrupt the double-diffusive microstructure. However, the lifespan of turbulent patches is rather short. When turbulence subsides, salt fingers reemerge, gain strength, and then continue to operate at near-equilibrium level until the next turbulent event wipes them out and the cycle repeats. There is a general consensus that the ability of salt fingers to effectively mix temperature and salinity in the ocean can be controlled by the frequency of turbulent disruptions.

Specific estimates of the impact of turbulence on fingers are more controversial and difficult to come by. The frequency of turbulent overturns can be roughly inferred from the so-called intermittency coefficient (I) which measures the fraction

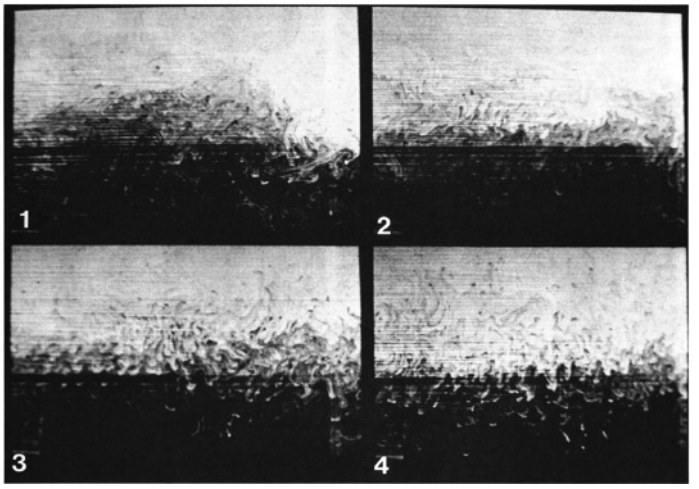

Figure 10.4 Dye fluorescence images of salt fingers establishing after a turbulent event. From Taylor (1991).

of the volume occupied by turbulence at any given time (Monin and Ozmidov, 1985). Observations indicate that the typical value of the intermittency coefficient in the main thermocline is $I \sim 0.05$ and its plausible range extends to $0.01 < I < 0.10$ (e.g., Polzin *et al.*, 2003). Numerical and laboratory experiments (Itsweire *et al.*, 1986, 1993) suggest that turbulence is suppressed on the time scale of one buoyancy period ($2\pi/N$), which leads to the following estimate of the period between subsequent turbulent events at a given location:

$$\Delta t \sim \frac{2\pi}{N}\frac{1-I}{I}. \tag{10.1}$$

It should be noted that this estimate assumes that bursts of turbulence are random in space and occur at comparable time intervals; both assumptions are readily questioned.

The period (10.1) should be compared with the time it takes for salt fingers to fully develop from the rubble left behind by turbulent overturns. Their recovery is by no means instantaneous. Figure 10.4 shows the reestablishment of salt fingers after turbulent disruption modeled in the laboratory by a grid falling through the tank (Taylor, 1991). Grid turbulence decayed rather rapidly ($t \approx 3.8/N$) giving way to wave motions. Salt fingers became visually detectable at $t \approx 10/N$, followed by an even longer period of growth and equilibration. It is intuitively clear that the recovery time for salt fingers (t_{rec}) is directly linked with their maximal growth rate (λ) and laboratory studies (Taylor, 1991; Wells and Griffiths, 2003) suggest

$$3\lambda^{-1} < t_{\mathrm{rec}} < 7\lambda^{-1}. \tag{10.2}$$

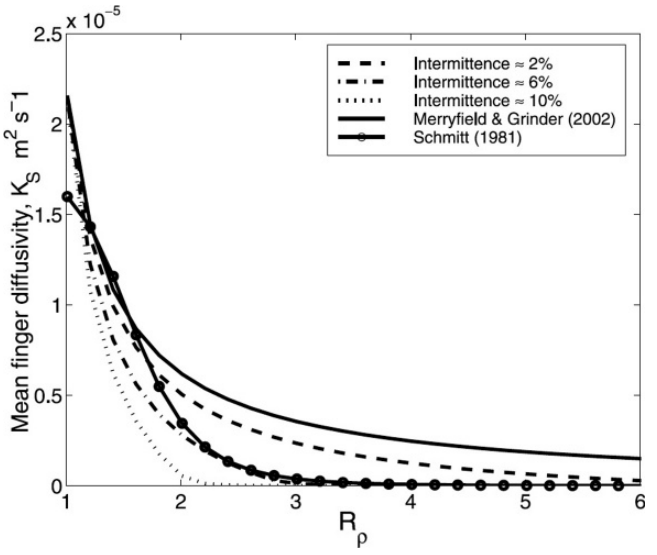

Figure 10.5 The time-averaged salt diffusivity due to fingers for typical oceanographic conditions. The intermittency of turbulent events varies in the range $2\% < I < 10\%$. The solid curve indicates the equilibrium diffusivity in the absence of turbulence and the curve with circles corresponds to the ad hoc parameterization of salt-finger diffusivities in Schmitt (1981). From Wells and Griffiths (2003).

If the recovery time (10.2) is much shorter than the periodicity of turbulence (10.1) then the mean finger-driven transport will be largely unaffected by the turbulence; otherwise it will be considerably reduced. The outcome is largely determined by two parameters: the intermittency coefficient I, controlling Δt, and the background density ratio R_ρ, which determines the growth rate of salt fingers and thereby t_{rec}. In order for salt fingers to remain active, both I and R_ρ have to be sufficiently low. For typical conditions in the Atlantic thermocline, $R_\rho \sim 2$ and $I \sim 0.05$, the ratio of the recovery/turbulence time scales in (10.1) and (10.2) is $\frac{t_{\text{rec}}}{\Delta t} \sim 0.1$ and therefore the effects of turbulence are relatively mild. However, this ratio can increase significantly for more (less) active turbulence (double-diffusion).

A more detailed theoretical analysis was performed by Wells and Griffiths (2003). Figure 10.5 shows time-mean eddy salt diffusivity (K_S) as a function of density ratio (R_ρ) in the absence of turbulent disruptions along with the equivalent relations for the cases of weak ($I = 0.02$), moderate ($I = 0.06$) and strong ($I = 0.1$) turbulence. The results in Figure 10.5 reveal high sensitivity of finger fluxes to the intensity of turbulence. Weak turbulence has only a secondary effect on salt fingers and could be largely ignored for most intents and purposes. The effects of moderate turbulence are, well, moderate. Strong turbulence, on the other hand,

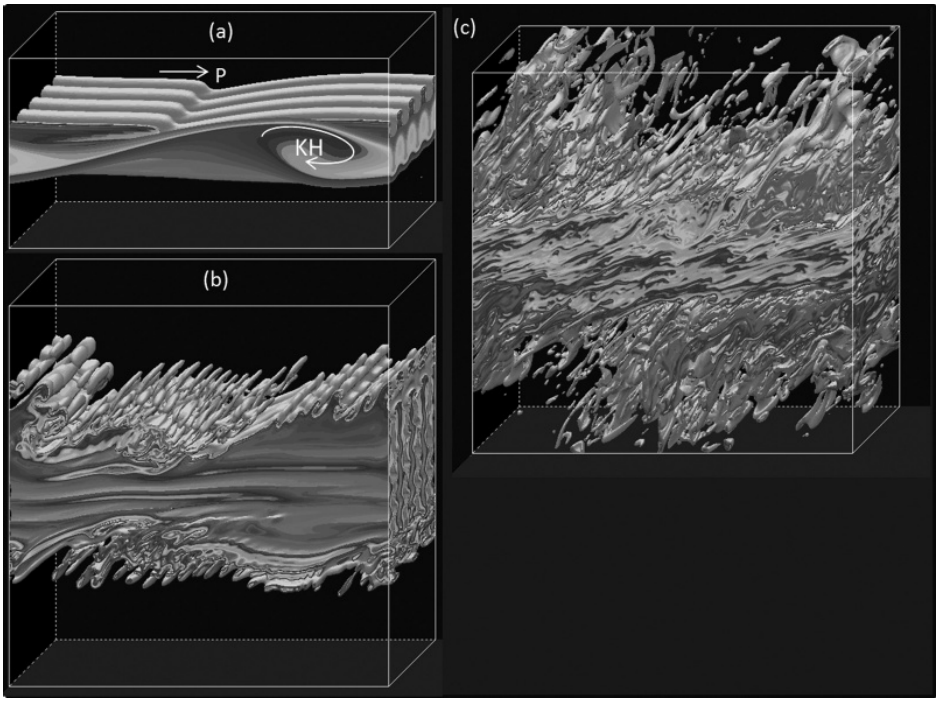

Figure 10.6 Salinity field from DNS of salt fingers in an unstable shear shown at various stages of evolution. From Smyth and Kimura (2011). See color plates section.

substantially diminishes K_S even for very active salt fingering ($R_\rho < 2$) and for $R_\rho > 2$ finger-induced mixing is all but eliminated.

The general picture of the fingers/turbulence interaction and even some specific predictions of the Wells and Griffiths' model are consistent with laboratory and numerical experiments. Laboratory studies have been performed in both heat–salt (Linden, 1971; Taylor, 1991) and salt–sugar (Wells and Griffiths, 2003) configurations; their evolutionary similarities can be taken as evidence of robust physics, independent of experimental media. Due to technical complications, laboratory finger/turbulence experiments have so far have been based exclusively on the grid-stirring method of turbulence production. A key strength of the numerical experiments, relative to their laboratory counterparts, lies in their ability to explicitly represent shear instabilities and the transition to turbulence. Despite substantial differences in setup, the simulated interaction of turbulence and fingers in many ways mirrors the lab experiments. The simulation in Figure 10.6 (Smyth and Kimura, 2011) was initiated by the dynamically unstable shear flow ($Ri = 0.18$) in the salt-finger favorable ($R_\rho = 2$) stratification. The first stage of the experiment is destabilization of the shear flow and formation of a turbulent Kelvin–Helmholtz

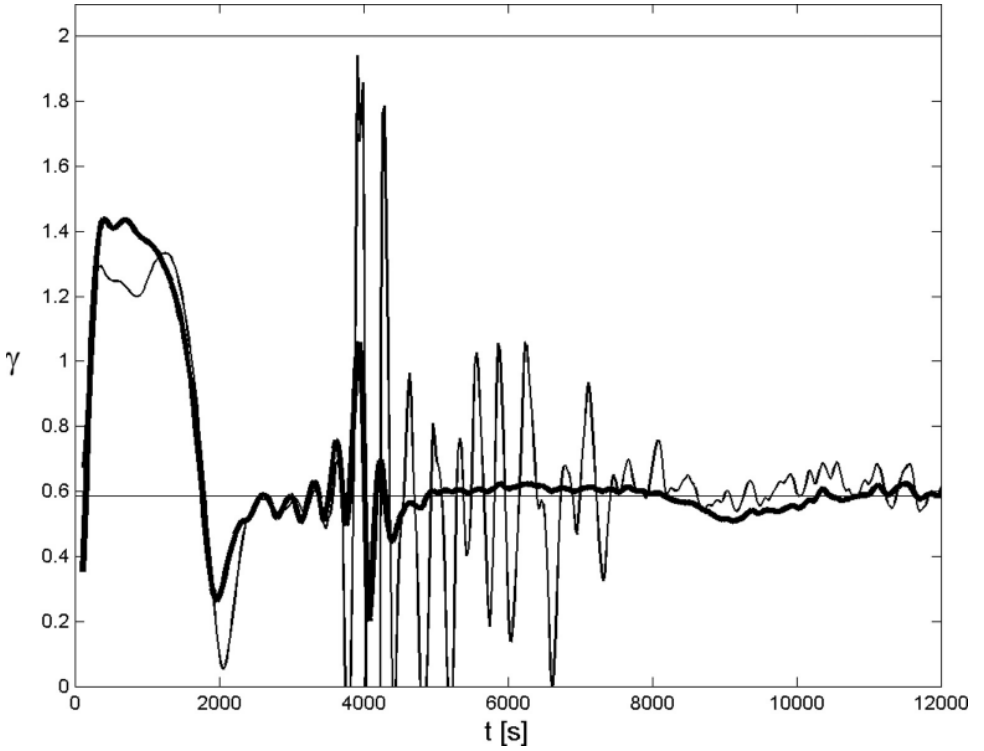

Figure 10.7 Flux ratio for the simulation in Figure 10.6. The thick curve is based on volume-averaged fluxes and the thin curve on fluxes at the centerline. Horizontal lines indicate the value for shear-driven turbulence ($\gamma = 2$) and for the fastest growing finger mode ($\gamma = 0.58$). From Smyth and Kimura (2011).

billow. The subsequent evolution of the system is characterized by the familiar, from lab studies, pattern of fingers/turbulence interaction – a brief period of active turbulence is followed by the more gradual growth and equilibration of fingers.

On the quantitative level, numerical experiments (Smyth and Kimura, 2011) tend to ascribe greater significance to finger transport than is typically seen in laboratory realizations. Despite the visually stunning appearance of turbulent overturns (Fig. 10.6) their direct contribution to the net mixing of temperature and salinity is considerably less than that of salt fingers. A convenient global indicator of the relative significance of fingers and turbulence is given by the heat/salt flux ratio (γ). The value expected for turbulence, which tends to mix temperature and salinity at equal rates, is $\gamma_{\text{turb}} = R_\rho = 2$, whilst for salt fingers it is $\gamma_{\text{sf}} \approx 0.6$. Figure 10.7 presents a time record of the flux ratio for the simulation in Figure 10.6. For the most part, γ hovers about the salt-finger value (γ_{sf}), never coming close to γ_{turb}. Even when turbulence is at its peak, it does not completely suppress fingering – a significant

difference relative to the laboratory experiments. Readers are also reminded of the simulations in which salt fingers interact with collective instability waves (Stellmach *et al*., 2011; Chapter 8, Fig. 8.18). After equilibration, these waves start to overturn, continuously generating random patches of turbulence, yet their impact on mixing is minimal (Fig. 8.18d). Such differences between laboratory and numerical predictions could reflect the significance of the method of turbulence production: grid-stirring experiments introduce a bias towards turbulence and simulations reproducing shear instability favor finger-driven mixing.

So far, our discussion has been focused on finger-driven fluxes and it should be emphasized that the effects of turbulence on the total *T*–*S* transports, which include both turbulent and finger components, are less pronounced. Turbulence suppresses salt fingers but contributes to vertical mixing on its own and therefore certain compensation is to be expected. Even the sign of the effect is not always clear. Depending on the particular experimental or environmental conditions, adding turbulence can increase, decrease or have little effect on the total transport. Linden's (1971) early laboratory experiments on the interaction of fingers with grid-generated turbulence revealed a weak non-monotonic dependence of the net salt flux on the frequency of turbulent disruptions. Elevated transports were found for predominantly fingering and predominantly turbulent regimes, and the net salt flux was minimal for comparable contributions from fingers and turbulence.

The role of turbulence in the mixing of density is less ambiguous. Double-diffusion is characterized by the counter-gradient (downward) density flux, whereas turbulence acts in the opposite sense, transporting density upward. Thus, taking turbulence into account increases the upward density flux through two distinct mechanisms: (i) by directly contributing to mixing and (ii) indirectly, by reducing the downward finger flux. Laboratory experiments (Wells and Griffiths, 2003) have demonstrated very clearly that, as the frequency of turbulent disruptions increases, the net density flux monotonically increases. The sign of this flux changes from negative in the finger-controlled regime to positive when turbulence dominates. Numerical simulations in which turbulence was generated by moderately unstable shear (Smyth and Kimura, 2011) are characterized by downward time-mean density flux, as expected for predominantly double-diffusive mixing. The instantaneous density flux, however, changes from slightly positive during the brief period of turbulent mixing to negative immediately after the decay of turbulence.

Needless to say, knowledge of the direction – never mind the exact value – of the vertical density transport in the thermocline is essential for many general oceanographic problems. The sign of density flux is controlled by the relative magnitudes of double-diffusive and turbulent mixing. Although both are still poorly constrained by observations, most of the evidence to date indicates that they are

comparable. Shear instabilities are violent and intense; they explode into a turbulent convective mess, which rapidly mixes temperature and salinity while the event lasts. In contrast, the instantaneous transport characteristics of salt fingers are relatively moderate. Nevertheless, double-diffusion contributes significantly to diapycnal mixing because the lower intensity of fingers is compensated by their continuous action during the long periods between turbulent events (Taylor, 1991). Time will tell of course, but it would not be surprising, for instance, to find an approximate cancellation of double-diffusive and turbulent density fluxes in the mid-latitude thermocline of the world ocean.

Regarding the large-scale implications of mixing, there is another critical point at stake. A number of modeling studies (e.g., Gargett and Holloway, 1992) reveal high sensitivity of large-scale circulation patterns to the ratio of turbulent diffusivities of heat and salt $r = K_T/K_S$. For many applications, this ratio matters even more than the magnitudes of K_T and K_S. In terms of expected values of r, double-diffusion and turbulence are very different. Turbulence tends to mix temperature and salinity at equal rates ($r_{\text{turb}} \approx 1$), whereas for salt fingers the turbulent diffusivity ratio is significantly lower, typically being restricted to the range $r_{\text{sf}} = \frac{\gamma_{\text{sf}}}{R_\rho} \sim 0.3{-}0.6$. Such a difference makes it imperative that the relative strengths of salt fingers and turbulence are quantified – only then will we have a chance of adequately representing small-scale mixing in ocean models. In the next section, we review the techniques used to discriminate between turbulence and salt fingers in oceanographic measurements.

10.4 Microstructure signatures of salt fingers in the ocean

The challenges involved in the detection, let alone the quantification and analysis, of salt fingers using ship-board measurements are obvious. Fingers are small scale and time dependent; they interact with shear and turbulence; they could be embedded in large-scale coherent structures, staircases and intrusions, but more often they are not. Yet, to provide the ultimate proof of importance, field measurements are essential. The ocean is an incredibly complex system and any unsubstantiated ivory-tower-theoretical attempt to assess the magnitude of double-diffusive mixing is likely to be met with suspicion.

Several qualitative methods of identifying double-diffusion in data have already been mentioned. Inferences could be made based on the values of density ratio, shadowgraph observations and the presence of steps in vertical temperature and salinity profiles. Unfortunately, all these signs are rather imprecise indicators of active double-diffusion. For instance, we can claim with some confidence that salt fingers play a substantial role in ocean mixing for $R_\rho < 2$ and that they are generally too weak to compete with turbulence for $R_\rho > 3$. This leaves vast regions of the

world ocean in the grey area where double-diffusion may or may not be important. The presence of well-defined staircases is sufficient to predict the dominance of double-diffusion but is far from necessary. Optical observations, which are yet to be included in the standard arsenal of microstructure measurements, can be effective in identifying salt fingers but offer little help in terms of quantifying their magnitude.

As difficult as the problem of identifying salt fingers in field measurements might be, the ocean gradually gives up its secrets. Numerous past successes and future prospects are associated with high-resolution O(cm) microstructure measurements. These methods were introduced more than forty years ago (Grant *et al*., 1968; Osborn and Cox, 1972) and have become progressively more sophisticated and accurate ever since. The two most common approaches to the detection of salt fingers in microstructure measurements involve the analysis of (i) spectral characteristics inferred from horizontally towed conductivity and temperature sensors and (ii) dissipation rates of kinetic energy and thermal variance.

Spectral characteristics

Salt fingering is a narrow-band phenomenon. This is a direct consequence of their dynamics; fingers are created and maintained by molecular dissipation. While much larger secondary structures (intrusions, collective instabilities and staircases) could be generated occasionally, the primary signal is tightly confined to the dissipative range – the energy enters and exits the system at comparable spatial scales. In this regard, turbulence is fundamentally different. A substantial separation between the forcing and dissipative scales, the presence of a broad inertial subrange, and the associated direct cascades of energy and tracer variances are the essential attributes of three-dimensional turbulence (Kolmogorov, 1941; Batchelor, 1959). The resulting distinction between the spectral imprints of fingers and turbulence has been profitably and extensively exploited to interpret microstructure measurements. Since the preferred width of salt fingers (unlike their vertical scale) can be readily evaluated on the basis of linear theory, spectral methods are particularly effective in the analysis of horizontal variability.

The first attempt of this nature was made by Magnell (1976), who analyzed conductivity fluctuations in a horizontal plane recorded by a towed microstructure instrument in the Mediterranean outflow. The Fourier spectrum of the conductivity record revealed a well-defined peak at wavenumbers closely corresponding to the fastest growing finger modes, which was readily interpreted as clear evidence of salt fingering. Of course, the double-diffusive origin of microstructure in the Mediterranean outflow could have been anticipated, given the low value of density ratio ($R_\rho \sim 1.3$) and the persistence of staircases. In contrast, the unique spectral

signatures of salt fingers detected in microstructure data from the North Pacific (Gargett and Schmitt, 1982) must have raised some eyebrows. Gargett and Schmitt analyzed the temperature record from a horizontally towed sensor and concluded that salt fingers operate in patchy regions with density ratios as high as $R_\rho \sim 3$. The limited-amplitude narrowband spectrum of temperature in these regions was markedly different from the broadband turbulent signal (Fig. 10.8a). Furthermore, the spectrum attributed to salt fingers was close to the prediction of the corresponding theoretical finger model (Fig. 10.8b), leaving little doubt in the interpretation of the microstructure signal.

The initial success of the spectral analysis of towed data stimulated numerous extensions. Marmorino (1987) used spectral analysis to identify fingers in the dataset obtained from towed fast-response conductivity sensors deployed in the Sargasso Sea. His conclusions matched those of Gargett and Schmitt (1982) – salt-finger patches are ubiquitous and, normally, could be distinguished from turbulent regions by characteristically narrowband spectra. A more detailed look at clear-cut instances of fingering microstructure (Fig. 10.9) reveals a very specific dependence of the conductivity gradient spectra on the wavenumber (k) on the low-k side: the power spectral density increases as k^2. Such dependence was observed in laboratory measurements (Taylor and Bucens, 1989) and in direct numerical simulations of salt fingers (Shen, 1993). Shen and Schmitt (1995) developed a simple model rationalizing the spectral slope of salt fingers from first principles. For turbulence, on the other hand, spectral slopes $\propto k$ are most common, which is consistent with classical turbulence theory (Batchelor, 1959). Such a definite distinction opened a very attractive opportunity to discriminate between fingers and turbulence on a quantitative, rather than a descriptive, level. A discriminant was badly needed to classify ambiguous cases of microstructure that possess features of both fingers and turbulence. The spectral slope of the temperature or conductivity gradient (S_L) held a promise of removing, or at least greatly reducing, the guesswork inevitable in the visual characterization of indistinct spectra.

An alternative approach was proposed by Holloway and Gargett (1987). These authors capitalized on a difference in the turbulent and fingering patterns of the probability density functions (PDFs) of tracers. Specific examples were presented for temperature fluctuations, although this technique could be applied just as easily to other measured quantities, such as conductivity or its gradient. The large signal variability and intermittence associated with turbulence are reflected in PDFs with relatively long tails. In fingering convection, on the other hand, fluctuations are restrained by secondary instabilities of salt fingers (Chapter 4) resulting in compact, nearly normal PDFs. For any measured quantity φ with zero mean value, the tightness of its PDF is conveniently measured by kurtosis $K = \frac{\langle \varphi^4 \rangle}{\langle \varphi^2 \rangle^2}$, which is

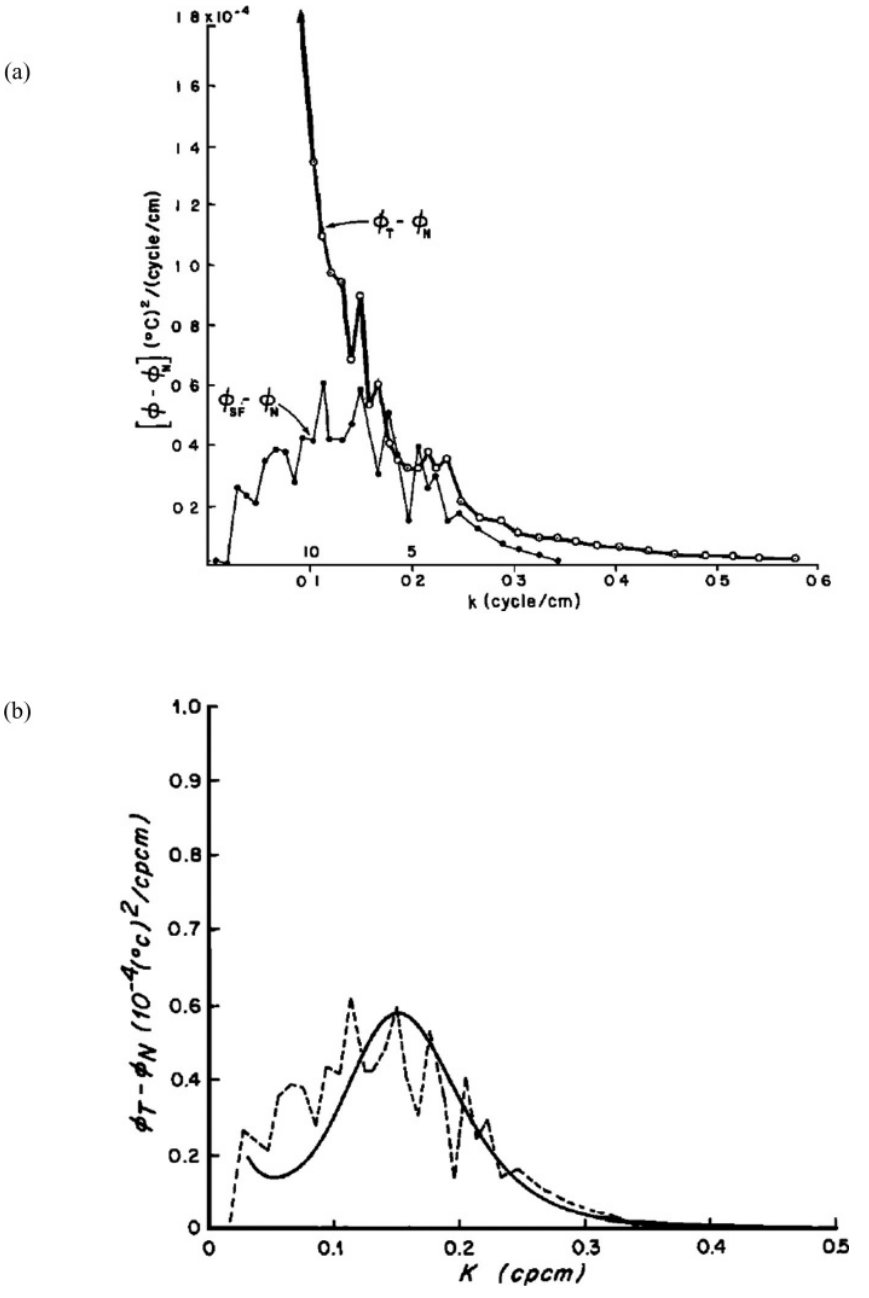

Figure 10.8 Spectral analysis of the temperature signal measured by a horizontally towed temperature sensor. (a) The horizontal temperature spectra show the limited bandwidth of the fingering signature and the characteristic dominance of the turbulent spectrum at low wavenumbers. (b) Comparison of the observed spectrum (dashed curve) with the corresponding theoretical model. From Gargett and Schmitt (1982).

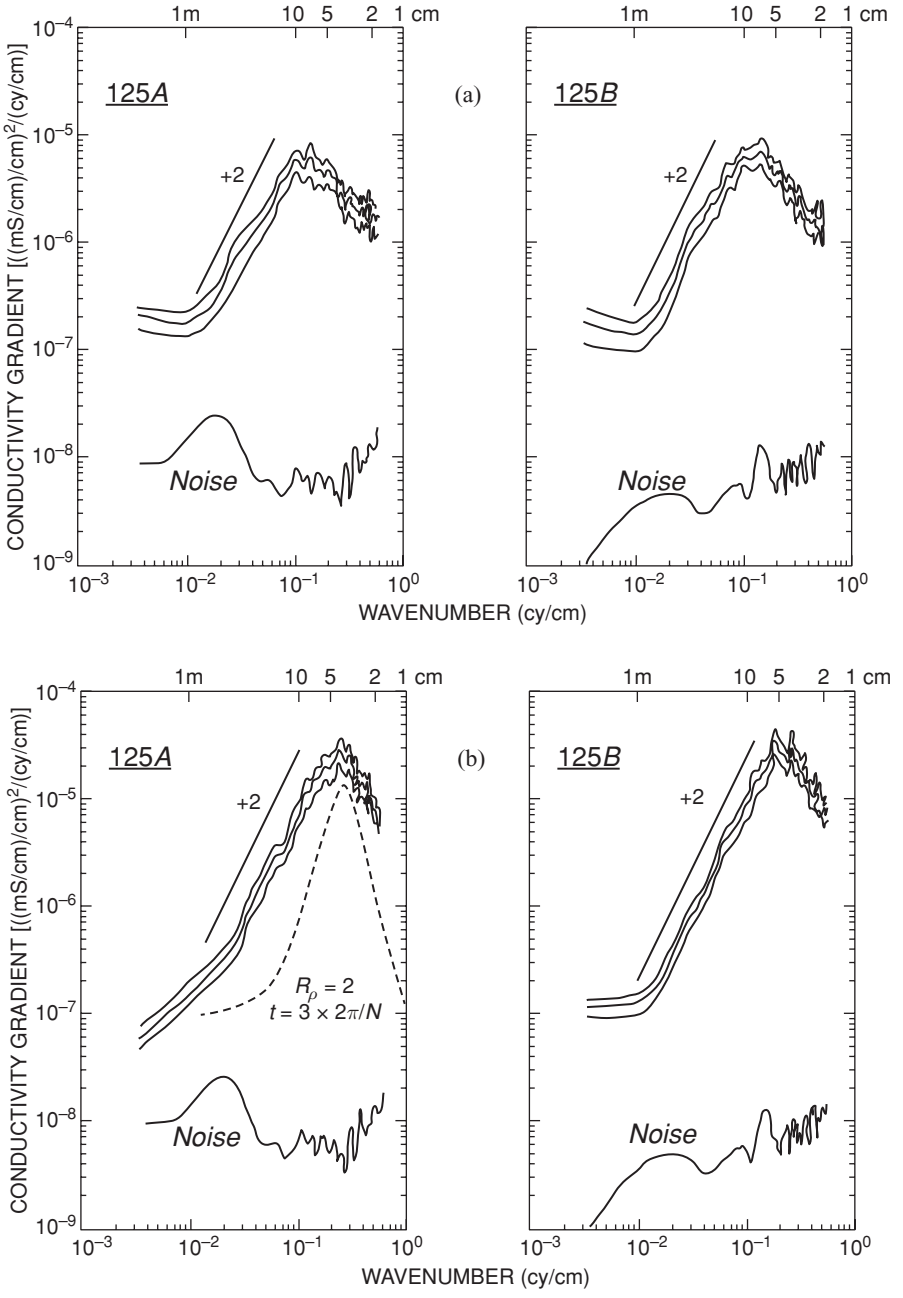

Figure 10.9 Conductivity gradient spectra from horizontally towed microstructure measurements in the regions of active fingering. Two different periods are analyzed in (a) and (b). The power spectral density increases as k^2 on the low-wavenumber side. Redrawn from Marmorino (1987).

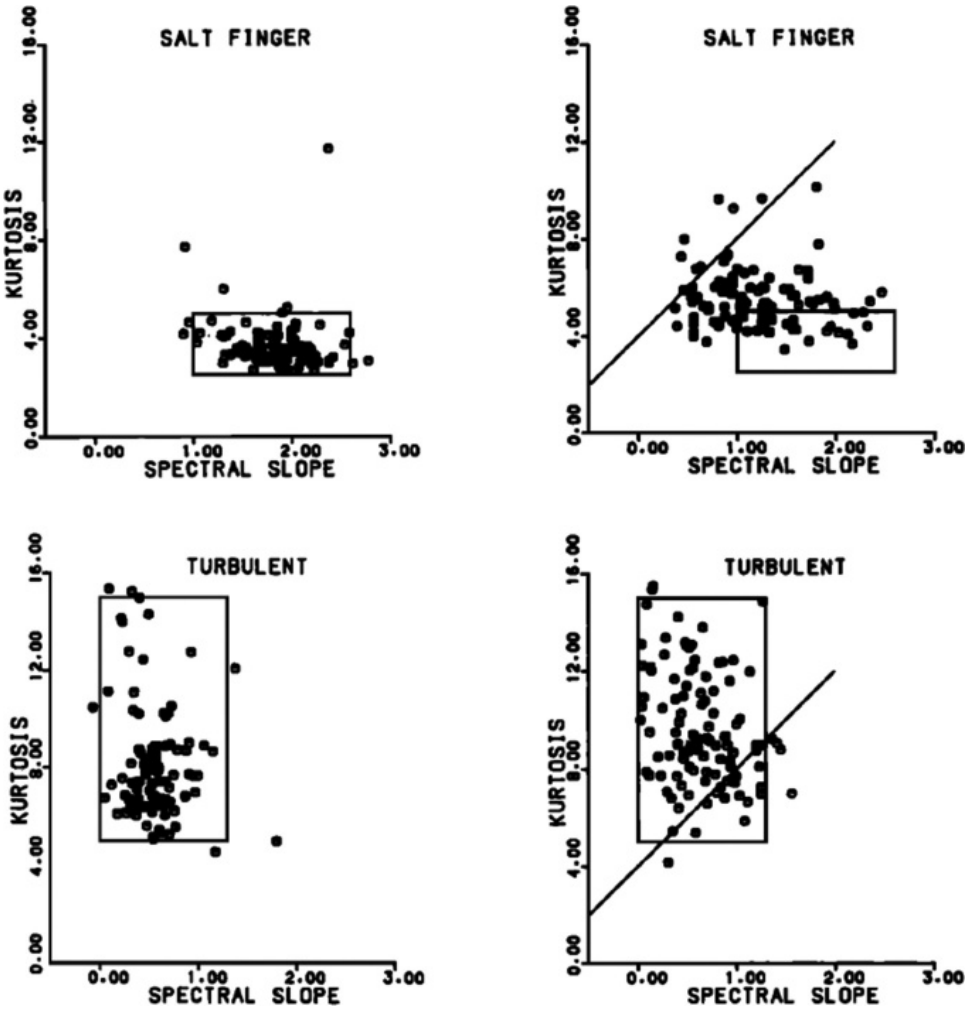

Figure 10.10 Scatter-plots of kurtosis versus spectral slope for data collected in the Sargasso Sea (right panel) and in the interfaces of the C-SALT staircase (left panel). Rectangles outline the Sargasso Sea populations for reference. The sloping line roughly divides the kurtosis–slope plane into fingering and turbulent populations. From Marmorino and Greenewalt (1988).

expected to be large for turbulence but low for fingers. Based on the analysis of unambiguous occurrences of fingers and turbulence, Holloway and Gargett suggested that $K_{\text{finger}} \sim 3$ and $K_{\text{turb}} \sim 7$.

The application of both kurtosis and slope diagnostics produced encouraging results. Figure 10.10 (Marmorino and Greenewalt, 1988) shows the scatter-plots of kurtosis (K) versus spectral slope (S_L) for data collected in the Sargasso Sea (right panel) and in the interfaces of the C-SALT staircase (left panel). Both

datasets indicate strong correlation between slope and kurtosis – low S_L, high K signal for turbulence; high S_L, low K for fingers – a sign of mutual consistency and efficacy of S_L-based and K-based methods of classification. Curiously enough, the Sargasso data were characterized by a very pronounced bimodal distribution of turbulent/finger signals, whereas the C-SALT interfaces apparently contained a significant fraction of mixed microstructure. To the best of our knowledge, no physical explanation for such a difference has yet been offered. The slope–kurtosis technique was further improved by Mack and Schoeberlein (1993), who combined these two quantities into a single optimal discriminator variable using the likelihood ratio (LLR) formalism of Whalen (1971). The LLR technique was shown to be more accurate than the S_L-based and K-based methods taken individually, allowing for a reliable classification of microstructure from towed data.

Analysis of dissipation measurements

While spectral techniques undoubtedly improved our ability to identify fingers and knowledge of their distribution, recent years have seen a shift to a different, logistically simpler and in many ways even more informative approach – an approach based on vertical profiling of the dissipation rates of kinetic energy (ε) and thermal variance (χ_T). Originally developed to quantify turbulent mixing (Osborn and Cox, 1972; Osborn, 1980), these methods were successfully adapted for finger-dominated and mixed environments (Oakey, 1988; St. Laurent and Schmitt, 1999). Concurrent measurements of ε and χ_T have become a standard component of field programs focused on diapycnal mixing, further motivating efforts to classify microstructure on the basis of dissipation signals. Dynamic dissimilarities of fingers and turbulence ultimately lead to different patterns of dissipation and several diagnostic models have successfully capitalized on such differences. The challenge lies in selection of the most general and least ambiguous criterion for interpreting the dissipation signals. The basics of the ε–χ_T diagnostic framework are reviewed next, followed by examples of its application to field measurements.

The first set of ideas that we wish to discuss is based on the energetics of fluid motion. The turbulent kinetic energy (TKE) budget, averaged in time and space over large (relative to the size and duration of a turbulent event) scales, is conveniently written (Osborn, 1980) as a balance between energy production (P), buoyancy flux (J_b) and molecular dissipation (ε):

$$P = J_b + \varepsilon. \tag{10.3}$$

The energy production term in (10.3) can be expressed as

$$P = -\overline{u_i' u_j'} \frac{\partial \bar{u}_i}{\partial x_j}, \; i, \, j = 1, 2, 3, \tag{10.4}$$

where $(x_1, x_2, x_3) = (x, y, z)$ and $(u_1, u_2, u_3) = (u, v, w)$. Vertical shears in the ocean greatly exceed the horizontal ones and therefore (10.4) reduces to

$$P = -\overline{u'w'} \frac{\partial \bar{u}}{\partial z} - \overline{v'w'} \frac{\partial \bar{v}}{\partial z}. \tag{10.5}$$

The vertical buoyancy flux in (10.3) is represented by

$$J_b = \frac{g}{\rho_0} \overline{\rho' w'}, \tag{10.6}$$

and the rate of loss of the kinetic energy to dissipation can be expressed as

$$\varepsilon = \frac{\nu}{2} \overline{\left(\frac{\partial u_i'}{\partial x_j} + \frac{\partial u_j'}{\partial x_i} \right)^2}. \tag{10.7}$$

Since most oceanographic measurements are one-dimensional, either horizontal or vertical, it is nearly impossible to evaluate (10.7) directly from data. The problem is often bypassed by assuming that microstructure is roughly isotropic at the dissipation scale. The accuracy of this approximation has been questioned repeatedly in both turbulent and double-diffusive contexts and there is a general consensus that the isotropic assumption could easily introduce an error in ε of a factor of two or so. Such an error can be tolerated in some studies, a-posteriori corrected in others, or – if you are particularly unlucky – it may also lead to questionable conclusions. There is more on this issue in the next section, but for now it is sufficient to say that the benefit of the isotropy assumption lies in the reduction of (10.7) to a more usable form:

$$\varepsilon \approx \varepsilon_V = \frac{15}{4} \nu \left(\overline{u_z'^2} + \overline{v_z'^2} \right). \tag{10.8}$$

The thee-way balance of the TKE (10.3) can be described using either the flux Richardson number

$$R_f = \frac{J_b}{P} = \frac{J_b}{J_b + \varepsilon}, \tag{10.9}$$

representing the ratio of potential energy gain to kinetic energy input, or the efficiency factor

$$\Gamma_e = \frac{J_b}{\varepsilon} = \frac{R_f}{1 - R_f}, \tag{10.10}$$

the ratio of potential energy gain to the kinetic energy loss. These quantities are sensitive to the type of microstructure and ultimately make it possible to distinguish between fingers and turbulence. Turbulence is driven by the energy released by the instabilities of the background flow, which is represented by the P-term in the TKE balance. Most of the energy input is dissipated by molecular viscosity and only a small fraction is converted into potential energy. Based on laboratory experiments at the time, Osborn (1980) suggested $R_f \leq 0.15$ and therefore $\Gamma_e \leq 0.2$. It has become common practice in oceanography to use Osborn's upper limit for the efficiency factor in turbulent events:

$$\Gamma_{e\,\mathrm{turb}} = 0.2, \tag{10.11}$$

and subsequent studies (Barry *et al*., 2001; Shih *et al*., 2005) confirmed that (10.11) offers a reasonable estimate for much of the relevant parameter range. Fingers, on the other hand, are driven by the release of potential energy stored in the salinity stratification, which renders the production term P inconsequential for their establishment and maintenance. In the limit $P \to 0$, the TKE balance reduces to $J_b = -\varepsilon$ or $\Gamma_{e\,\mathrm{fingers}} = -1$.

The second component of the diagnostic framework, which to some extent mirrors the treatment of the TKE budget, is based on the temperature variance equation (Osborn and Cox, 1972). After averaging in time and space, this equation reduces to the balance between the variance production by the large-scale flow and molecular dissipation:

$$-2\overline{u_i' T}\frac{\partial \bar{T}}{\partial x_i} = \chi_T, \tag{10.12}$$

where the dissipation term is given by

$$\chi_T = 2k_T\overline{\left(\frac{\partial T'}{\partial x_i}\right)^2}. \tag{10.13}$$

The production term in (10.12) represents the effects of both lateral ($i = 1,2$) and vertical ($i = 3$) advection. Lateral advection can be essential for variance production in frontal regions with sharp horizontal temperature gradients, which often harbor pronounced intrusive structures (see Chapter 7). However, in much of the ocean, lateral gradients are relatively weak and the production of thermal variance is dominated by its vertical component, which reduces (10.12) to

$$-2\overline{w'T'}\frac{\partial \bar{T}}{\partial z} = \chi_T. \tag{10.14}$$

In order to evaluate (10.14) from one-dimensional microstructure measurements, the isotropic assumption is invoked once again:

$$\chi_T \approx \chi_{TV} = 6k_T\overline{\left(\frac{\partial T'}{\partial z}\right)^2}, \tag{10.15}$$

which reduces the temperature variance equation to

$$-\overline{w'T'}\frac{\partial \bar{T}}{\partial z} \approx 3k_T\overline{\left(\frac{\partial T'}{\partial z}\right)^2}. \tag{10.16}$$

The simplified integral budgets of TKE (10.3) and temperature variance (10.16) form the foundation of the microstructure diagnostic methods. They provide an explicit link between the dissipation characteristics (which are measurable) and the vertical fluxes of heat, density and momentum (which affect the large-scale dynamics of the ocean). While it is straightforward to formulate a similar budget for the salinity variance, it would be of limited utility since technical complications currently preclude direct measurements of salt dissipation (χ_S). It should be mentioned though that there is a significant interest in the technology that would make it possible to infer χ_S from data (e.g., Nash and Moum, 1999) and the prospects of developing sensors capable of measuring salinity microstructure are very real.

The question now arises of how to use the production–dissipation balances to discriminate between turbulence and fingers. Fluid dynamics is a science of non-dimensional numbers and the selection of the most appropriate ones is vital for the success of any diagnostic model. For the background large-scale flow, the two relevant non-dimensional parameters are the density ratio and Richardson number; the former indicating propensity for fingering, the latter for turbulence. Criteria used to characterize the microstructure signals are more complex and the choices are less obvious.

A non-dimensional measure of temperature dissipation is given by the Cox number:

$$Cx_T = \frac{1}{\bar{T}_z^2}\overline{\left(\frac{\partial T'}{\partial x_i}\right)^2} = \frac{\chi_T}{2k_T\bar{T}_z^2}, \tag{10.17}$$

which, in view of (10.14), reduces to the Nusselt number (Nu) used throughout this monograph. The physical interpretation of the Cox number is straightforward – it measures the relative magnitudes of the eddy and molecular diffusivities of temperature:

$$K_T = Cx_T k_T. \tag{10.18}$$

Salt fingers and turbulence in the thermocline are typically characterized by comparable Cox numbers (Cx_T = 10–100). This rules out Cx_T as an effective

discriminator between fingers and turbulence, although it can be conveniently used to quantify the intensity of small-scale mixing.

A non-dimensional number often invoked to characterize the dissipation of kinetic energy is the buoyancy Reynolds number:

$$Re_b = \frac{\varepsilon}{\nu N^2}. \tag{10.19}$$

Unlike the Cox number, Re_b does offer some insight into the origin of microstructure. Turbulence is an ineffective mixer – (10.11) implies that the energy lost to frictional dissipation is much higher than the energy invested directly into the vertical transport of properties. Frictional dissipation due to fingers, on the other hand, is very limited. The typical values of the flux ratio $\gamma \sim 0.6 - 0.7$ mean that the rate at which potential energy is gained by temperature stratification exceeds the frictional loss. Thus, for comparable rates of temperature mixing – as measured by Cx_T, χ_T, or K_T – turbulence has much stronger expression in terms of ε and therefore higher values of Re_b. Inoue *et al.* (2007) capitalized on this property to identify finger-dominated microstructure in the Oyashio/Kuroshio/Tsugaru currents system. The key element of the diagnostic model was the criterion $Re_b < 20$ ($Re_b > 20$) for fingers (turbulence). This criterion was supplemented by a set of necessary conditions: mixing was assumed significant only for $\chi_T > 5 \cdot 10^{-9}\,^{\circ}\mathrm{C}^2\,\mathrm{s}^{-1}$ and microstructure was classified as fingering only for $1 < R_\rho < 3$ and $0 < \gamma < 1$. The estimated diffusivities for finger-dominated regions were consistent with the expected salt-finger patterns and in reasonable agreement with extant parameterizations (Zhang *et al.*, 1998). While the Re_b-based criterion is expected to perform well under typical conditions, the possibility exists for misclassification of microstructure in the extreme cases of anomalously low-amplitude turbulence or high-amplitude fingering.

The most effective and widely used approach to classification of microstructure combines measurements of ε and χ_T into a single discriminator variable known as the dissipation ratio:

$$\Gamma = \frac{\chi_T N^2}{2\varepsilon \bar{T}_z^2}. \tag{10.20}$$

This method is based on exactly the same principle as the Re_b-based criterion – frictional loss of energy in turbulent flows is much higher than in fingering regions. Hence, the dissipation ratio should be low for turbulence and high for fingers. This statement can be made more precise as follows. Turbulence mixes temperature, salinity and density at approximately the same rate $K_{T\,\mathrm{turb}} = K_{\rho\,\mathrm{turb}}$ or, equivalently,

$$\frac{\overline{w'T'}}{\bar{T}_z} = \frac{\overline{w'\rho'}}{\bar{\rho}_z} = \frac{J_b}{N^2}. \tag{10.21}$$

Drawing together (10.10), (10.14) and (10.21), we reduce (10.20) to

$$\Gamma_{\text{turb}} = \Gamma_{e\,\text{turb}} \sim 0.2. \tag{10.22}$$

Thus, the dissipation ratio in purely turbulent flows is identical to the efficiency factor. This property often leads to the indiscriminate usage of the terms "dissipation ratio" and "efficiency factor" in microstructure literature – the same variable (Γ) is often assigned for both quantities. All this may be acceptable if the topic is limited to turbulence. However, the lack of firm conventions could lead to confusion in discussions of double-diffusive or mixed microstructure. To eliminate the risk of misinterpretation, it is important to emphasize the principal differences between the efficiency factor and the dissipation ratio. The primary definition of the dissipation ratio (10.20) is based on the dissipation signals. The efficiency factor quantifies the TKE balance and it is unambiguously defined by (10.10). Purely turbulent events aside, the dissipation ratio (Γ) and efficiency factor (Γ_e) are different, numerically and conceptually, and should be treated as such.

For the case of pure fingering, the dissipation ratio can be explicitly evaluated (e.g., Hamilton *et al.*, 1989) by assuming that the production term (P) in the TKE budget is negligible and

$$J_b \equiv g\frac{\overline{w'\rho'}}{\rho_0} = -\varepsilon. \tag{10.23}$$

Breaking down the density flux into its components $F_T = \overline{w'T'}$ and $F_S = \gamma^{-1}F_T = \gamma^{-1}\overline{w'T'}$ simplifies (10.23) to

$$g\alpha\left(\gamma^{-1} - 1\right)\overline{w'T'} = -\varepsilon. \tag{10.24}$$

Combining (10.24) with (10.16), we express the dissipation ratio (10.20) in terms of the flux ratio and the density ratio, whose values are relatively well constrained:

$$\Gamma_{\text{finger}} = \frac{N^2}{\bar{T}_z g\alpha\left(\gamma^{-1} - 1\right)} = \frac{1 - R_\rho^{-1}}{\gamma^{-1} - 1}. \tag{10.25}$$

Thus, for typical values of $R_\rho \sim 2$ and $\gamma \sim 0.6 - 0.7$, we expect $\Gamma_{\text{finger}} \sim 1$, which is considerably higher than the turbulent value (10.22).

The credit for the first application of the criterion $\Gamma_{\text{finger}} > \Gamma_{\text{turb}}$ to data goes to Oakey (1988), who analyzed profiler measurements of ε and χ_T through meddy Sharon. Oakey reported several incidences of unusually high dissipation ratio ($\Gamma > 1$), which invariably occurred in regions with double-diffusively favorable stratification – a clear sign of the efficacy of the Γ-based classification method. McDougall and Ruddick (1992) further developed this approach by proposing an algorithm to infer the salinity flux from microstructure data. The first step involves

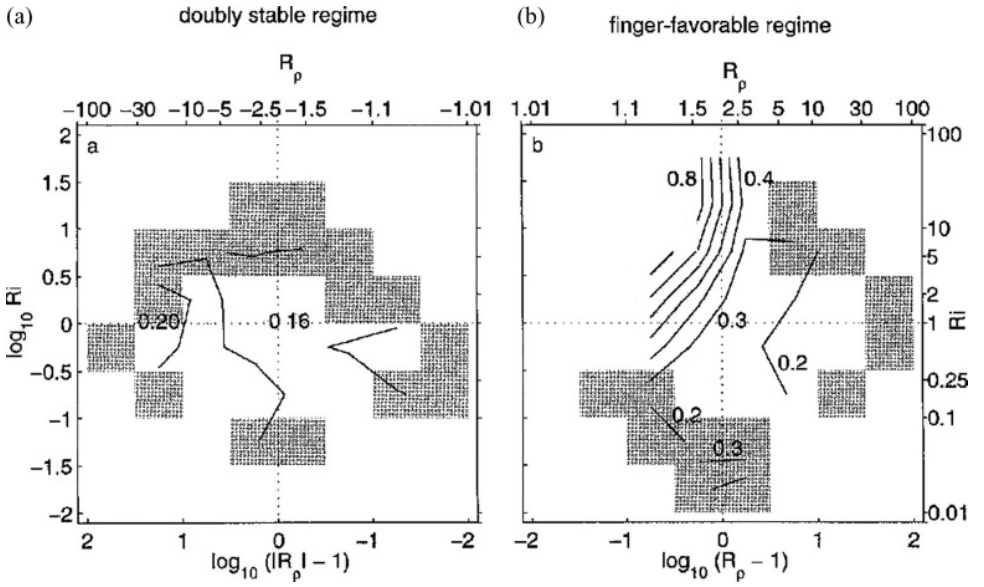

Figure 10.11 The variation of the dissipation ratio (Γ) as a function of the Richardson number (Ri) and the density ratio (R_ρ) in (a) double-diffusively stable and (b) salt-finger favorable regimes. Regions of darker shading denote bins where the uncertainty in Γ exceeds 25% of the mean. The finger-favorable regime is characterized by the elevated dissipation ratios, particularly in the $1 < R_\rho < 2$, $Ri > 1$ region of parameter space. From St. Laurent and Schmitt (1999).

estimation of the relative contributions of fingers and turbulence to mixing from the position of the observed dissipation ratio Γ_{obs} within the interval $\Gamma_{\text{turb}} < \Gamma < \Gamma_{\text{finger}}$. Knowledge of the composition of microstructure, in turn, makes it possible to determine both the temperature and salinity fluxes from ε and χ_T. The technique was shown to be reasonably accurate; the errors in the inferred salt and heat fluxes are primarily associated with the uncertainty in the assumed finger flux ratio. Since direct measurement of salinity microstructure is currently beyond our technological capabilities, the diagnostics of the salt flux, singularly afforded by the McDougall and Ruddick method, proved to be most valuable for the analysis of mixed microstructure.

A definitive test of the Γ-based approach was performed by St. Laurent and Schmitt (1999). These authors examined the extensive microstructure dataset from the site of the North Atlantic Tracer Release Experiment (NATRE). The NATRE area is only moderately favorable to fingering and is actively turbulent, which presents a major challenge for reliable detection and quantification of finger-induced mixing. Nevertheless, St. Laurent and Schmitt were able to discern the salt-finger signal by focusing on the statistics of the dissipation ratio. The exploration of the two-dimensional parameter space of density ratio and Richardson number (R_ρ, Ri) was particularly informative in this regard (Fig. 10.11). The range

$1 < R_\rho < 2, Ri > 1$ (weak turbulence, strong fingers) was characterized by elevated values of Γ, which are consistent with the finger model (10.25) and cannot be attributed to turbulence (10.22). Outside of this parameter region, the dissipation ratio was low and better described by the turbulence model.

St. Laurent and Schmitt (1999) also inferred the diffusivities of heat and salt (K_T and K_S) from the NATRE microstructure data using methodology analogous to that of McDougall and Ruddick (1992). The results revealed a significant difference between the average values of K_T and K_S in the region – a difference that is caused entirely by fingers:

$$K_T = 0.8 \cdot 10^{-4}\,\mathrm{m^2\,s^{-1}},\ K_S = 1.3 \cdot 10^{-4}\,\mathrm{m^2\,s^{-1}}. \tag{10.26}$$

The microstructure-based estimate of K_S in (10.26) is remarkably close to the tracer diffusivity

$$K_{\mathrm{tracer}} = 1.2 \cdot 10^{-4}\,\mathrm{m^2\,s^{-1}} \tag{10.27}$$

evaluated from the vertical spreading of a passive chemical (sulfur hexafluoride) released during NATRE. The actual eddy diffusivity of the tracer is expected to be equal to that of salt because their molecular diffusivities are close. In this regard, the agreement between (10.26) and (10.27) is encouraging. It supports inferences based on microstructure analysis and emphasizes the significance of double-diffusive mixing in the presence of active turbulence.

In summary, the microstructure diagnostics discussed in this section provide irrefutable evidence of vigorous fingering in much of the upper ocean. Particularly promising are the methods based on the concurrent measurements of ε and χ_T, which carry the twin benefits of (i) classifying the microstructure as finger-dominated or primarily turbulent and (ii) making it possible to evaluate the vertical diffusivities of temperature, salinity and momentum. A questionable aspect of the dissipation-based methods is the assumed isotropy of microstructure, commonly invoked to infer three-dimensional dissipation from one-dimensional measurements. The ramifications of the anisotropic effects and the prospects for reduction of the associated error are discussed next.

Anisotropy of salt fingers

At first, the idea of resorting to an isotropic model of microstructure, particularly in the context of salt fingers, appears to be overly simplistic and unwarranted. Most double-diffusive theories picture salt fingers as anisotropic and vertically oriented (e.g., Holyer, 1984; Kunze, 1987). Even the name "salt finger" immediately conveys the sense of an elongated structure, something that perhaps should not be modeled as a round eddy. In reality, the effects of anisotropy are rather moderate. The microstructure estimates of vertical transport – the estimates based on the isotropic

model – are generally consistent with the tracer release measurements. This has been demonstrated for the staircase (Schmitt *et al.*, 2005) and smooth-gradient (St. Laurent and Schmitt, 1999) regimes, which suggests that anisotropic effects are limited. Of course, since tracer- and microstructure-based estimates are indirect, one cannot dismiss the possibility that both methods may be biased and the agreement is, to some extent, fortuitous. Furthermore, even if the isotropic model does not lead to major inconsistencies, the anisotropy should be quantified and an effort made to reduce the associated error.

While the conceptual theory of finger anisotropy is noticeably missing, several attempts have already been made to quantify the effect. Taylor (1993) conducted a series of laboratory experiments aimed at determining the aspect ratio of salt fingers and examining its variation with the density ratio. The operational definition of the aspect ratio was based on the dominant vertical and horizontal wavelengths of temperature spectra. The average aspect ratio for $R_\rho < 5$ was found to be 0.58, which means that fingers are about twice as long as they are wide. Taylor noted the systematic trend of salt fingers to become more isotropic at low values of the density ratio, with the aspect ratio approaching unity for $R_\rho \to 1$. These results are consistent with the *in situ* oceanic measurements of salt fingers by a horizontally towed device (Lueck, 1987). Lueck found very little coherence between the temperature records of two sensors vertically separated by 6 cm – a distance comparable to the dominant scale of primary salt-finger instability at the observational site. The lack of vertical coherence supports the isotropic model of salt fingers.

Numerical studies (e.g., Shen, 1989; Stern *et al.*, 2001) repeatedly challenged the notion of long vertical fingers, particularly at low density ratios ($R_\rho < 2$). An important step was made by Caplan (2008), who used DNS to evaluate and correct the systematic bias in the profiler approximation of dissipation quantities. Salt-finger experiments with various density ratios were diagnosed to evaluate the actual dissipation ε and χ_T, given in (10.7) and (10.13) respectively, as well as the dissipation inferred from the vertical profiles (ε_V and χ_{TV}) in (10.8) and (10.15) using the isotropic approximation. The difference between the actual and inferred dissipation was expressed in terms of anisotropic coefficients A_{VV} and A_{TV} such that

$$A_{VV} = \frac{\varepsilon}{\varepsilon_V} = \frac{\sum_{i,j} \frac{1}{2} \overline{\left(\frac{\partial u_i'}{\partial x_j} + \frac{\partial u_j'}{\partial x_i} \right)^2}}{\frac{15}{4} \nu \left(\overline{u_z'^2} + \overline{v_z'^2} \right)}, \quad A_{TV} = \frac{\chi_T}{\chi_{TV}} = \frac{\overline{\sum_i \left(\frac{\partial T'}{\partial x_i} \right)^2}}{3 \overline{\left(\frac{\partial T'}{\partial z} \right)^2}}. \tag{10.28}$$

The results of the anisotropy analysis were suggestive. The anisotropic coefficient for temperature was sufficiently close to unity ($1 < A_{TV} < 1.3$), which

implies that the profiler approximation offers a fairly accurate estimate of χ_T. The profiler approximation of ε is more problematic. The anisotropic coefficient for TKE monotonically increased from $A_{VV} = 1.3$ at $R_\rho = 1.1$ to $A_{VV} = 2.0$ at $R_\rho = 1.9$. Such high values of A_{VV} imply that the profiler approximation could quite significantly, by as much as a factor of two, underestimate the rates of TKE dissipation. The anisotropy characteristics of salt fingers in two- and three-dimensional simulations were similar – a sign of the robust dynamics of the processes controlling anisotropy. To estimate the error introduced by the isotropic approximation in the analysis of towed microstructure data, Caplan (2008) also diagnosed the horizontal anisotropy coefficients $A_{VH} = \frac{\varepsilon}{\varepsilon_H}$ and $A_{TH} = \frac{\chi_T}{\chi_{TH}}$. The horizontal coefficients conveyed the same message: salt fingers can be considered roughly isotropic for the purpose of evaluating χ_T but significant error is to be expected for ε. A suggestion was made to reduce the anisotropy-related errors of the data-based dissipation estimates by incorporating the anisotropy coefficients, recorded as a function of R_ρ, in post-processing of microstructure measurements. Caplan's anisotropy analysis was extended to the DNS of fingers in a sheared background flow by Kimura *et al.* (2011), who found that laminar shear has a relatively minor effect on the anisotropy coefficients.

10.5 Inverse modeling of thermohaline staircases

This chapter would be deplorably incomplete without mentioning one more method of evaluating double-diffusive transport in the ocean – the inverse modeling of thermohaline staircases (Lee and Veronis, 1991; Veronis, 2007). This method is yet to receive the level of attention given to microstructure-based and tracer-release studies or, for that matter, the level of attention it deserves. Nevertheless, the technique is promising. In view of the success of inverse modeling in other branches of oceanography and beyond (e.g., Bennett, 2002), we can safely assume that its future applications will constrain estimates of mixing in staircases and generate new insights into their dynamics.

Inverse models attempt to calculate the unknown model parameters by fitting measurements to the governing equations in a manner that minimizes the suitably defined integral error. Lee and Veronis (1991) used the 1985 C-SALT dataset for the Caribbean staircase, which was particularly appropriate for inversion. The steps in the staircase were steady and well-defined. The observations were regularly spaced, making this dataset ideal for discretization. The governing equations were taken to be the temperature and salinity advection–diffusion equations in divergence form:

$$\nabla_H (\vec{v}_H C) + \frac{\partial (wC)}{\partial z} = \frac{\partial}{\partial z}\left(K_C \frac{\partial C}{\partial z} \right), \tag{10.29}$$

where subscript H refers to horizontal components and C may be T or S, and the continuity equation

$$\nabla_H \vec{v}_H + \frac{\partial w}{\partial z} = 0. \tag{10.30}$$

The governing equations were vertically integrated over each layer and discretized by staggering all variables in space in the form of an Arakawa C grid (Fig. 10.12). The result is finite-difference forms of (10.29) and (10.30), which were applied to each of the six layers and sixteen horizontal locations in the central part of the staircase indicated in Figure 10.12. The temperature, salinity and depth of each layer at observational locations were treated as known variables, velocities and diffusivities as unknown. After discretization, the linear homogeneous governing system reduced to

$$\mathbf{A} \cdot \vec{\mathrm{X}} = 0, \tag{10.31}$$

where $\vec{\mathrm{X}}$ is the vector of unknowns and $\mathbf{A}$ is the matrix that contains the coefficients of these unknown variables in the finite-difference tracer and continuity equations. In order to complete the inversion, the system was cast in inhomogeneous form by dividing all the equations by an arbitrarily chosen reference unknown X_r, and rewriting (10.31) as

$$\mathbf{A}^* \cdot \vec{\mathrm{X}}^* = \vec{b}, \tag{10.32}$$

where $\vec{\mathrm{X}}^*$ is a vector consisting of relative unknowns. In Lee and Veronis' model, (10.32) represented an over-determined system of 288 equations with 260 unknowns and its best-fit solution was determined using the method of total least squares (Golub and van Loan, 1983). The solution, of course, was only for the relative unknowns and therefore all original unknowns ($\vec{X}$) were determined up to a constant factor – the complication that stems from the homogeneous nature of the governing equations (10.29) and (10.30). At this point, the inversion yielded the ratios of unknowns but not their absolute values. For instance, the inversion was remarkably successful in predicting the flux ratio:

$$\gamma_{\mathrm{inv}} = \frac{K_T}{K_S} R_\rho = 0.89 \pm 0.07, \tag{10.33}$$

which closely matched the estimate based on the lateral density ratio in C-SALT layers, $\gamma \approx 0.85$ (Schmitt *et al.*, 1987).

However, the inversion remained incomplete without invoking some additional consideration that would make it possible to normalize the unknowns. The original study (Lee and Veronis, 1991) made use of the horizontal velocity measurements by a current meter at one of the stations during C-SALT. While this seemed a reasonable solution at the time, the resulting diffusivities were unrealistically high,

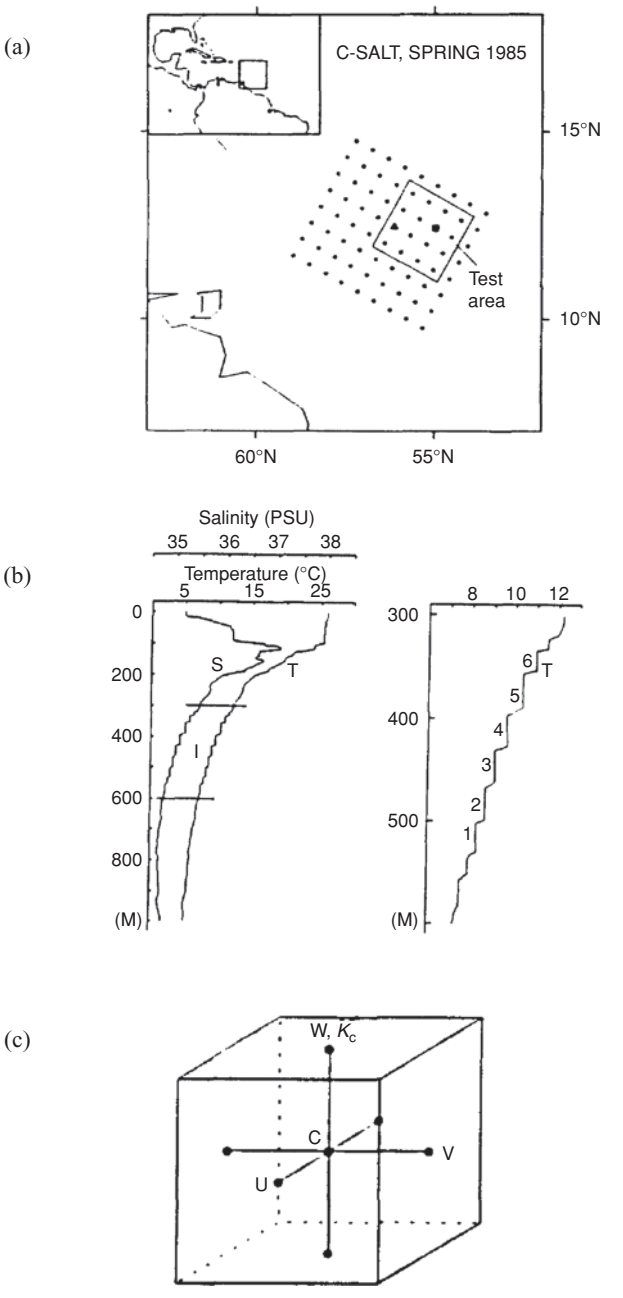

Figure 10.12 Inverse model of the Caribbean staircase. (a) The map of the survey region in C-SALT; the inverse model is applied to the 4 × 4 array in the boxed area. (b) The left panel presents the vertical *T*–*S* profiles at the location marked by a solid square in (a). The section of the temperature profile that contains the six layers used for the inversion is shown in the right panel. (c) The seven-point grid used for discretization of the governing equations. From Lee and Veronis (1991).

casting some doubt on the inversion procedure. The root cause of the problem was identified much later by Veronis (2007). The isotherms, isohalines and isopycnals in the C-SALT region are close due to the tightness of the T–S relation in the double-diffusive thermocline. Therefore, the governing equations (10.29) are largely invariant with respect to the changes in velocity component directed along isopycnals. Thus, the inversion reliably predicts only the flow component normal to the isopycnals but not the full velocity, which means that the horizontal velocity cannot be used to pin down the magnitudes of the unknowns. Incidentally, the same invariance property of the T–S equations resulted in yet another complication. When Lee and Veronis attempted to include the geostrophic momentum equations in the governing system, the solutions became inconsistent. In retrospect, it is clear that the failure of the combined system is related to the fundamental differences in the structure of the tracer and geostrophic equations, the former being controlled by the diapycnal and the latter by isopycnal velocity components.

The problem of finding an appropriate constraint for the inversion is a serious one. If the horizontal velocity cannot be used to complete the inversion, then what can? Fortunately, a simple remedy has been found. Veronis (2007) recalibrated the inversion data using the value of the Ekman pumping velocity in the C-SALT region as a proxy for the mean vertical velocity and obtained the following estimates of the mean diffusivities in the staircase:

$$K_{T\mathrm{inv}} = 0.47 \cdot 10^{-4}\,\mathrm{m^2\,s^{-1}} \text{ and } K_{S\mathrm{inv}} = 0.89 \cdot 10^{-4}\,\mathrm{m^2\,s^{-1}}. \qquad (10.34)$$

The inversion-based diffusivities came very close to the microstructure-based prediction $K_{T\mathrm{micr}} = 0.45 \cdot 10^{-4}\,\mathrm{m^2\,s^{-1}}$ and $K_{S\mathrm{micr}} = 0.85 \cdot 10^{-4}\,\mathrm{m^2\,s^{-1}}$ (Schmitt *et al*., 2005). The estimate (10.34) is also consistent with the salt diffusivity $K_{S\mathrm{tr}} = (0.8 - 0.9) \cdot 10^{-4}\,\mathrm{m^2\,s^{-1}}$ inferred from the spreading of a passive tracer released in the central part of the Caribbean staircase, which brings the whole story to a very satisfying resolution. While the inversion, tracer and microstructure based methods have their own limitations and their individual predictions could be questioned, the agreement of all three cannot be coincidental. The actual diffusivities are likely to be somewhere in the vicinity of (10.34). The only estimate that significantly deviates from (10.34) is based on application of the laboratory-calibrated 4/3 flux law to the Caribbean staircase, which yields much higher diffusivities: $K_{S\,\mathrm{lab}} \sim 6 \cdot 10^{-4}\,\mathrm{m^2\,s^{-1}}$ (e.g., Lambert and Sturges, 1977). As discussed earlier, the elevated values of $K_{S\,\mathrm{lab}}$ are readily attributed to very different conditions in the ocean and laboratory. Thus, on the basis of the observational estimates of fluxes in staircases we can conclude that (i) double-diffusion is the dominant mixing agent, (ii) the vertical T–S transport can only be evaluated using methods that are fully

compatible with the double-diffusive nature of the phenomenon, and (iii) the active oceanic environment adversely affects double-diffusive mixing in staircases.

And to conclude this chapter, here is a final thought for not-so-mature readers like myself. Why is finger transport lower in the ocean than in the laboratory? Because the ocean always keeps its fingers crossed.